

Article

Numerical Investigation of the Heat Transfer Characteristics of R290 Flow Boiling in Corrugated Tubes with Different Internal Corrugated Structures

Shenglin Zhu ^{1,2}, Jinfeng Wang ^{1,2,3,4,*}  and Jing Xie ^{1,2,3,4,*} 

¹ College of Food Science and Technology, Shanghai Ocean University, Shanghai 201306, China; m190300696@st.shou.edu.cn

² Shanghai Professional Technology Service Platform on Cold Chain Equipment Performance and Energy Saving Evaluation, Shanghai 201306, China

³ Shanghai Engineering Research Center of Aquatic Product Processing & Preservation, Shanghai 201306, China

⁴ National Experimental Teaching Demonstration Center for Food Science and Engineering, Shanghai Ocean University, Shanghai 201306, China

* Correspondence: jfwang@shou.edu.cn (J.W.); jxie@shou.edu.cn (J.X.)

Abstract: The heat transfer and pressure drop characteristics of R290 flow boiling in a corrugated tube were investigated through computational fluid dynamics (CFD) in this study. We established a model of flow boiling in a corrugated tube with different corrugated structures (rectangular and circular corrugations) and validated the model using the Liu–Winterton and Xu–Fang empirical equations. The heat transfer coefficient (HTC) and pressure drop were obtained at a mass flow rate of 0.04–0.2 kg/s and a water inlet temperature of 310–330 K. The results show that the HTC and the drop in the pressure of the corrugated tubes both obviously increased compared with a smooth tube as the mass flow rate increased. The HTC decreased for the three tubes as the water inlet temperature increased, while the drop in pressure slightly increased for the three tubes. Moreover, the corrugated structure was found to significantly enhance the heat transfer; the heat transfer enhancement factor (E_1) of the corrugated tube with the rectangular corrugations and the corrugated tube with the circular corrugations was 2.01–2.36 and 1.67–1.98, respectively. The efficiency index (I) for both the rectangular corrugated pipe and the circular corrugated pipe was greater than 1 (1.05–1.24 and 1.13–1.29, respectively). The application of corrugated tubes with round and rectangular corrugations can reduce the heat transfer area required for the exchange of heat and, thus, reduce the cost.

Keywords: R290; flow boiling; numerical simulation; heat transfer; corrugated tube



Citation: Zhu, S.; Wang, J.; Xie, J. Numerical Investigation of the Heat Transfer Characteristics of R290 Flow Boiling in Corrugated Tubes with Different Internal Corrugated Structures. *Mathematics* **2021**, *9*, 2969. <https://doi.org/10.3390/math9222969>

Academic Editor: Arturo Hidalgo

Received: 31 October 2021

Accepted: 20 November 2021

Published: 21 November 2021

Publisher's Note: MDPI stays neutral with regard to jurisdictional claims in published maps and institutional affiliations.



Copyright: © 2021 by the authors. Licensee MDPI, Basel, Switzerland. This article is an open access article distributed under the terms and conditions of the Creative Commons Attribution (CC BY) license (<https://creativecommons.org/licenses/by/4.0/>).

1. Introduction

The destruction of the ozone layer and greenhouse gas pollution are becoming increasingly serious and are environmental issues of global concern. Energy savings and emissions reductions have become the main measures used to solve these problems. According to the Montreal and Kyoto Protocols and a series of agreements, the HCFC and HFC refrigerants currently in general use should be gradually phased out due to their disadvantages, such as destruction of the atmosphere and aggravation of the greenhouse effect [1]. R290 (propane) has an Ozone Depletion Potential (ODP) of 0, a Global Warming Potential (GWP) of 20, a density of $580 \text{ kg}\cdot\text{m}^{-3}$, and the advantages of being non-toxic, chlorine-free, and low in carbon. Its key thermophysical properties, such as its boiling point, freezing point, and critical point, are similar to those of R22, and it has excellent recyclability and is environmentally friendly; therefore, it is an ideal alternative refrigerant [2–5]. However, the application of R290 is limited due to the disadvantages of its flammability and explosiveness [6]. Consequently, the heat exchanger structure needs to be properly optimized. The use of enhancement tubes with a small diameter provides an

opportunity to reduce the size of heat exchangers by enhancing the heat transfer, which, in turn, can reduce the refrigerant charge of R290 to within the safe use range [7,8].

The flow boiling of R290 in tubes has mainly been studied in smooth microchannels. Nguyen et al. [9] studied the effect of the mass flux, the heat flux, the saturation temperature, and the refrigerant vapor's quality on the heat transfer coefficient of R290 in a smooth tube with a diameter of 1.5 mm. Zhou et al. [10] studied the effect of the mass flux, the heat flow density, and the saturation temperature on the heat transfer coefficient and drop in pressure of R290 in smooth tubes with a diameter of 6 mm, 8 mm, and 10 mm and found that the heat flux and mass flux have an obvious impact on the coefficients. de Oliveira et al. [11] determined the heat transfer coefficients and studied the flow patterns during the flow boiling of propane in a tube with an inner diameter (ID) of 1 mm. The results showed that the HTC had a significant influence on the mass flux and heat flux. Lillo et al. [7] conducted experiments to evaluate the two-phase flow boiling heat transfer coefficient and dry-out incipient vapor quality of R290 in a tube with a 6 mm ID under different operating conditions.

Passively enhanced heat transfer technology is currently the most promising method for improving the heat transfer performance of heat exchangers. A rough surface is one of the techniques for passively enhancing the heat transfer. For decades, finned tubes [12,13], coiled tubes [14], inserts [15,16], and corrugated tubes [17–22] have been extensively studied. The effects of enhanced geometries on the heat transfer of boiling refrigerants have been addressed in several studies. Diani [23] examined the HTC for the evaporation of R513A in smooth and microfinned tubes with a diameter of 3.5 mm. The results showed that the microfinned tubes considerably augmented the HTC, especially at a low mass velocity. Celen et al. [24] conducted experiments to study the evaporation of R134a in smooth and microfinned tubes and found that the HTC was increased by 1.9 times while the pressure drop was increased by 3 times. Colombo et al. [25] investigated the flow patterns and characteristics of the evaporation and condensation of R134a in a smooth tube and two microfinned tubes and found an increase in the HTC for both microfinned tubes compared with the smooth tube. Allymehr [6] experimentally observed characteristics of the evaporation of R290 in smooth and microfinned tubes with a diameter of 5 mm and found a significant increase in the HTC for both microfinned tubes compared with the smooth tube. Previous studies were devoted to the investigation of refrigerant flow boiling in microfinned tubes. Fewer studies have been conducted on R290 flow boiling in corrugated tubes.

The purpose of this paper is to study the characteristics of R290 flow boiling in corrugated tubes. We used corrugated and smooth tubes with an inner diameter of 5 mm. The HTCs and drop in pressure were determined at a refrigerant mass flow rate of between 0.04 and 0.2 m/s and a water inlet temperature ranging from 310 to 330 K. In addition, the HTCs and drop in pressure of the smooth tube were measured at saturation temperatures ranging from 273 to 283 K. The results of this study could lead to the effective design of compact heat exchangers and the application of R290 in compact heat exchangers.

2. Numerical Simulation Procedures

2.1. Physical Model

The two types of corrugated structures of the corrugated pipe are shown in Figure 1. The corrugated tube consists of two coaxial tubes with convex corrugations on the internal wall of the inner pipes. The corrugation is of two types: rectangular and circular corrugations. The length and inner diameter of the tubes (the corrugated and smooth tubes) were kept at 300 mm and 5 mm, respectively. The corrugation height (Hl), tube-wall thickness (tl = 0.2 mm), corrugation width (wl), and corrugation pitch (pl) of the corrugated tubes are listed in Table 1.

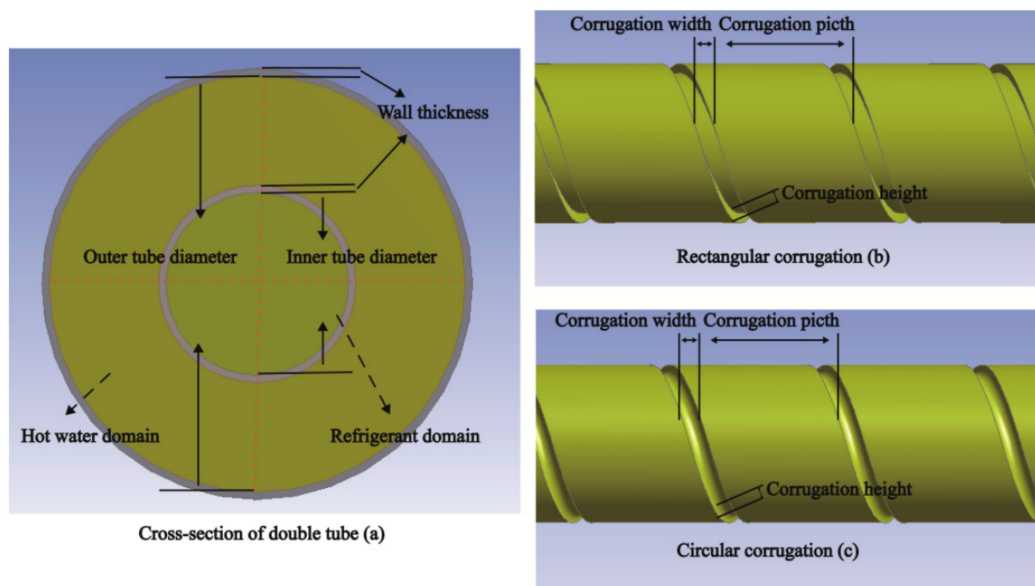


Figure 1. Configurational parameters of the corrugated tubes.

Table 1. Dimensions of the corrugated tubes.

Case	Inner Diameter (ID, mm)	Height (H, mm)	Pitch (P, mm)	Width (W, mm)	H/D	P/D
1	5	0.3	5	0.6	0.06	0.5
2	5	0.3	5	0.6	0.06	1
3	5	0.3	5	0.6	0.06	1.4

2.2. Governing Equations

In the numerical simulation of fluid flow, the velocity of the fluid is calculated by continuity and momentum equations. The temperature field of the fluid is evaluated by an energy equation. The flow boiling and heat transfer characteristics in corrugated pipes were studied by using the mixture multiphase flow model and the standard k-ε turbulence model. The numerical simulations were performed in ANSYS Fluent 19.0.

The mixture model is a simplified multiphase model that can be used in various ways. When the mixture model is used to simulate a multiphase flow, the phases move at different velocities, but a local equilibrium is assumed on a short spatial length scale. Homogeneous multiphase flows with a very strong coupling and with each phase moving at the same velocity are suitable for simulation using the mixture model. The continuity equation, the momentum equation, and the energy equation for the mixed phase and the volume fraction of the second phase are included in the mixture model [26,27].

The continuity equation is as follows:

$$\partial(\rho_m)/\partial t + \nabla \cdot (\rho_m \vec{v}_m) = 0 \tag{1}$$

where

$$\vec{v}_m = \sum_{k=1}^n \alpha_k \rho_k \vec{v}_k / \rho_m \tag{2}$$

and

$$\rho_m = \sum_{k=1}^n \alpha_k \rho_k \tag{3}$$

where \vec{v}_m refers to the mass average velocity, ρ_m refers to the mixture density, α_k refers to the kth phase volume fraction, ρ_k refers to the kth phase density, and \vec{v}_k refers to the kth phase velocity vector.

The momentum equation is as follows:

$$\partial(\rho_m \vec{v}_m) / \partial t + \nabla \vec{v}_m \cdot (\rho_m \vec{v}_m) = -\nabla P_m + \nabla \cdot [\mu_m \nabla \vec{v}_m^T] + \rho_m \vec{g} + \vec{F} + \nabla \cdot (\sum_{k=1}^n \alpha_k \rho_k \vec{v}_{dr,k} \vec{v}_{dr,k}) \tag{4}$$

where

$$\mu_m = \sum_{k=1}^n \alpha_k \mu_k \tag{5}$$

and

$$\vec{v}_{dr,k} = \vec{v}_k - \vec{v}_m \tag{6}$$

where \vec{F} refers to the bulk force, μ_m refers to the mixture viscosity, P_m refers to the mixture pressure, μ_k refers to the kth phase viscosity, h_k refers to the gravity, and $\vec{v}_{dr,k}$ refers to the kth phase drift velocity vector.

The energy equation is as follows:

$$\partial \left(\sum_{k=1}^n \alpha_k \rho_k E_k + P \right) / \partial t = \nabla \cdot (k_{eff} \nabla T) + S_E \tag{7}$$

where

$$E_k = h_k - P / \rho_k + v_k^2 / 2 \tag{8}$$

where K_{eff} refers to the effective thermal conductivity, P refers to the pressure, h_k refers to the kth sensible enthalpy, and S_E refers to the energy source term of all phases.

The second-phase volume fraction equation is as follows:

$$\partial(\alpha_v \rho_v) / \partial t + \nabla \cdot (\alpha_v \rho_v \vec{v}_m) = -\nabla \cdot (\alpha_v \rho_v \vec{v}_{dr,v}) + m_{lv} \tag{9}$$

where

$$\vec{v}_{qp} = \vec{v}_p - \vec{v}_q \tag{10}$$

where \vec{v}_{qp} refers to the relative velocity of the different phase, \vec{v}_p refers to the velocity of the secondary phase, \vec{v}_q refers to the velocity of the primary phase, and m_{lv} refers to the source term for the interacting mass conversion from the liquid to the vapor phase.

The standard k-ε turbulence model with the standard near-wall treatment was chosen. There is a standard k-ε model that is based on the transport equation of turbulent kinetic energy (k) and its dissipation rate (ε). It is assumed in the derivation of the k-ε model that the flow is completely turbulent and the effect of molecular viscosity is negligible [26]. The equations are:

$$\partial \rho(k) / \partial t + \partial(\rho k \mu_i) / \partial x_i = \partial \left[\left(\alpha_k \mu_{eff} \right) \frac{\partial h}{\partial x_j} \right] / \partial x_i + G_k + G_b - \rho \epsilon - Y_M + S_k \tag{11}$$

and

$$\partial(\rho \epsilon) / \partial t + \partial(\rho \epsilon \mu_i) / \partial x_i = \partial \left[\left(\alpha_\epsilon \mu_{eff} \right) \frac{\partial \epsilon}{\partial x_j} \right] / \partial x_i + C_{1\epsilon}(G_k + G_{3\epsilon} G_b) \epsilon / k - C_{2\epsilon} \rho \epsilon^2 / k + S_\epsilon \tag{12}$$

where G_k refers to the kinetic energy of the turbulence that is generated by the average velocity gradient, G_b refers to the kinetic energy of the turbulence that is generated by buoyancy, Y_M refers to the overall dissipation rate, which is generated by the fluctuating

expansion of the compressible turbulent flow, k refers to the turbulent pulsation kinetic energy, ε refers to the turbulent pulsation kinetic energy dissipation rate, S_k and S_ε refer to user-defined source terms, and $C_{1\varepsilon}$, $C_{2\varepsilon}$, and $C_{3\varepsilon}$ refer to constants. Some constants for the k - ε turbulence model are shown in Table 2.

Table 2. Coefficients for the standard k - ε turbulence model.

$C_{1\varepsilon}$	$C_{2\varepsilon}$	C_μ	σ_k	σ_ε
1.44	1.92	0.09	1.0	1.3

2.3. Boundary Conditions and Numerical Method

The boundary conditions and algorithm settings of the model were as follows (a–g).

- The simulation model utilized velocity-inlet and pressure-outlet conditions;
- The coupling boundary was adopted for the inner tube wall and the adiabatic boundary was adopted for the outer tube wall. Copper is the material of the tube wall;
- The viscosity, thermal conductivity, density, and specific heat of each phase of the fluid were constant, and the latent heat and surface tension of the fluid were also constant;
- The impact of surface tension was considered in the model, and the “implicit body force” was selected in the mixture model. In the model, the first and second phases were the liquid phase and the vapor phase of R290, respectively. The third phase was water;
- The governing equations were solved by the steady-state implicit format;
- In the simulation algorithm, SIMPLE was selected for the pressure–velocity coupling and QUICK was selected to be used for the volume fraction equation. For the energy, volume, and turbine kinetic energy equations, a first-order upwind scheme was used;
- Convergence was achieved for the energy variable up to 10^{-6} and for the other variables (continuity, x-velocity, y-velocity, z-velocity, k , epsilon, volume fraction—R290 vapor, volume fraction—water) up to 10^{-3} .

2.4. Grid Independence Check

The meshing process was conducted with ANSYS Mesh 19.0 using the unstructured grid. The refined grid was placed near the wall to ensure that the variations in temperature and velocity were captured at the wall. Different views of the mesh are presented in Figure 2. To examine the independence of the numerical results from the number of elements, the value of the heat transfer coefficient was investigated using 1.1–15.14 million elements. From Figure 3, the effect of the number of elements on the results can be ignored after 5.96 million grids. In addition, the numerical simulation results using 5.96 million grids have an error of 0.9% compared with those using 15.14 million grids. Therefore, in order to reduce the number of computations, the grid number of 5.96 million was chosen for the numerical calculations.

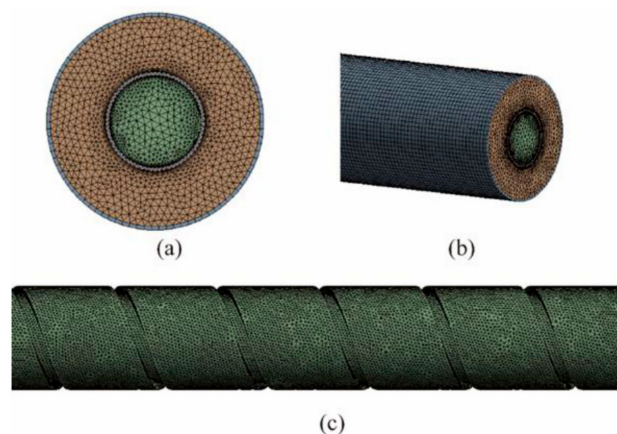


Figure 2. Grid structure of the corrugated tube.

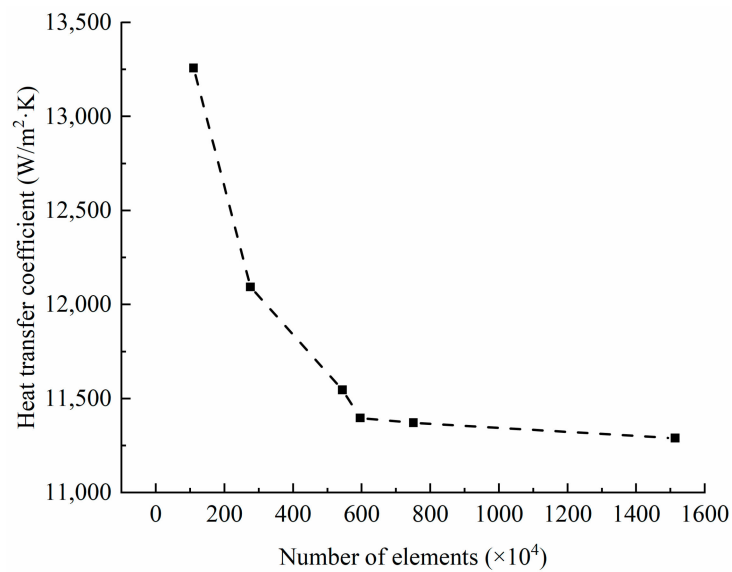


Figure 3. Heat transfer coefficient of the corrugated pipe with different numbers of elements.

2.5. Model Verification

A total of 5.96 million elements were selected to perform the numerical calculations, and the numerical simulation results were verified by experimental results. The results of the CFD-based HTC were evaluated by the empirical correlation as shown in Figure 4. The water inlet temperature was kept at 320 K and the refrigerant inlet temperature was kept at 282 K. The R290 mass flow rate was changed from 0.04 to 0.2 kg/s. The HTC and pressure drop of the inner tube for the smooth tube were used as parameters to validate the model. A maximum deviation of 8.96% with the Liu–Winterton empirical equation [28] was observed for the surface heat transfer coefficient. A maximum deviation of 9.09% with the Xu–Fang empirical equation [29] was observed for the pressure drop.

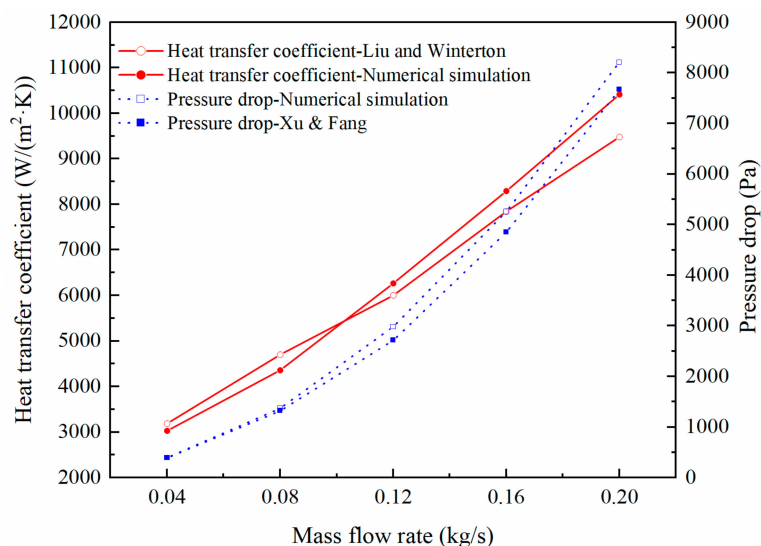


Figure 4. Validation of numerical simulation results with empirical correlations.

The Liu–Winterton empirical equation is as follows:

$$H_3 = \left[(E_f H_2)^2 + (S_f H_1)^2 \right]^{0.5} \tag{13}$$

where H_3 refers to the transfer heat coefficient; E_f refers to the forced convection heat transfer enhancement factor; S_f refers to the suppression factor; $E_f H_2$ refers to the forced convection mechanism's contribution; and $S_f h_1$ refers to the contribution of the nucleate boiling mechanism. H_2 is calculated by Equation (14) and H_1 is calculated by Equation (15).

$$H_2 = 0.023 Re^{0.8} Pr^{0.4} \lambda_l / D \quad (14)$$

where Pr is the Prandtl number; Re is the Reynolds number; λ_l is the liquid's thermal conductivity; and D is the inner diameter.

$$H_1 = 55 P_f^{0.12} \left(-\log_{10} P_f \right)^{-0.55} M^{-0.5} Q^{0.67} \quad (15)$$

where the molecular weight and heat flux are represented by M and Q , respectively. P_f is the reduced pressure (absolute pressure/critical pressure)

$$E_f = [1 + Pr(\rho_l/\rho_v - 1)]^{0.35} \quad (16)$$

where ρ_l and ρ_v are the liquid density and the vapor density, respectively. Pr is the Prandtl number.

$$S_f = \left(1 + 0.055 E_f^{0.1} Re^{0.16} \right)^{-1} \quad (17)$$

where v_l represents the liquid's velocity and μ_l represents the liquid's dynamic viscosity.

The Xu–Fang empirical equation is as follows:

$$\Delta P = L f m^2 / 2ID\rho \quad (18)$$

$$f = 0.25 \left[\log \left(150.39 / Re^{0.98865} - 152.66 / Re \right) \right]^{-2} \quad (19)$$

where L and ID refer to the tube length and diameter, respectively. m represents the liquid mass flux and ρ_l is the liquid density.

3. Results and Discussion

The influence of saturation temperature with respect to the HTC and pressure drop for the smooth tube is illustrated in Figure 5. As the saturation temperature increases from 273 K to 283 K, the HTC is increased by about 4.8%, while the pressure drop is decreased by about 8.96%. The saturation temperature has a certain impact on the nucleate boiling area, but only a small impact on the convection area. This is explained by the fact that the bubble generation rate depends mainly on the thermophysical properties of the fluid at the same temperature. The variation in the pressure drop is also mainly attributed to the different thermophysical properties of the fluid because of the different saturation temperatures. Due to the small range of variation in the saturation temperature, the thermophysical properties of the fluid have very small variations. Therefore, the saturation temperature has a slight impact on the HTC and pressure drop [6]. No specific numerical simulations were conducted in the corrugated tubes to evaluate the impact of saturation temperature.

3.1. Heat Transfer Coefficient

The HTC calculation equation is

$$H = Q / T_w - T_{sat} \quad (20)$$

where Q refers to the thermal flux, T_w refers to the wall temperature, and T_{sat} refers to the fluid saturation temperature.

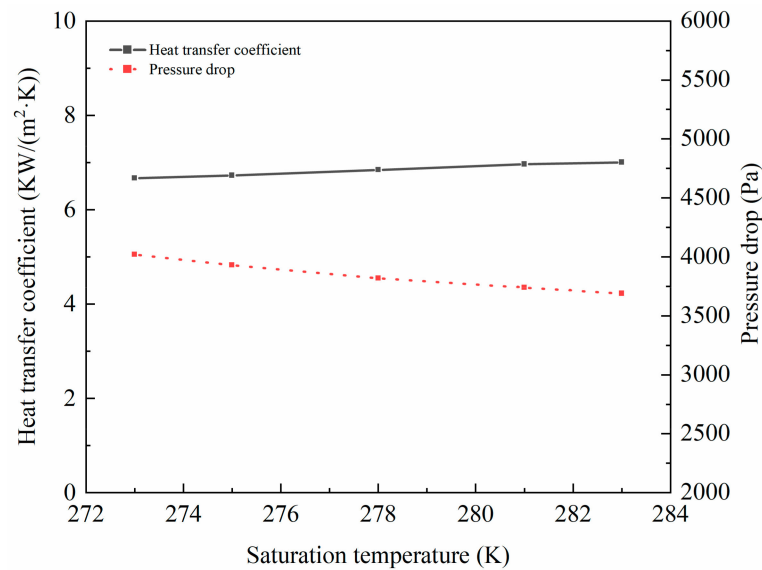


Figure 5. Impact of saturation temperature on the HTC and pressure drop of the smooth tube.

3.1.1. Mass Flow Rate

The impact of the R290 mass flow rate with respect to the local HTC in the three different tubes is shown in Figure 6. The local HTC increases as the R290 mass flow rate increases and increases along the channel with distance. The R290 vapor volume fraction increases along the tube with distance. The R290 vapor's velocity increases as the volume fraction of the vapor increases. This improves the apparent velocity of the vapor phase, reinforces the interference between the vapor and the liquid at the interface, and facilitates a more vigorous mixing flow. Therefore, both phenomena facilitate the enhancement of convective boiling and can explain the enhanced heat transfer. Compared with the smooth tube, both corrugated tubes show a significant increase in the HTC. The HTCs of corrugated pipes with round corrugations and corrugated pipes with rectangular corrugations are 66.8–98.5% and 101.4–135.7% higher than those of smooth pipes, respectively. This phenomenon can be explained from two perspectives. On the one hand, the fluid aggregates in the inner corrugated structure, resulting in the creation of the secondary flow. The turbulent kinetic energy (TKE) at the inner spiral of the corrugated structure is significantly higher than at other locations because of the generation of the secondary flow as shown in Figure 7. A higher TKE indicates a higher degree of turbulence. The TKE at the rectangular corrugation is higher than that at the circular corrugation as seen in Figure 7. Consequently, the heat transfer is enhanced, and the rectangular corrugation enhances the heat transfer more significantly. On the other hand, the inner tube wall temperature has a significant influence on the generation and detachment of bubbles. A corrugated structure provides surface area for the transfer of heat, resulting in a higher wall temperature of the corrugated pipes compared with smooth pipes. From the Clausius–Clabellon equation, it is known that nucleation sites are more likely to form on a corrugated structure. Consequently, the heat transfer is enhanced at boiling temperature. This phenomenon is more obvious in corrugated pipes whose corrugations are rectangular. For the same heat transfer rate, the required heat transfer area of corrugated tubes with circular and rectangular corrugations is 66.8–98.5% and 101.4–135.7% less than that of smooth tubes, respectively. Therefore, the use of corrugated tubes provides an opportunity to reduce the sizes of the heat exchangers and to reduce the R290 charge in the heat exchangers.

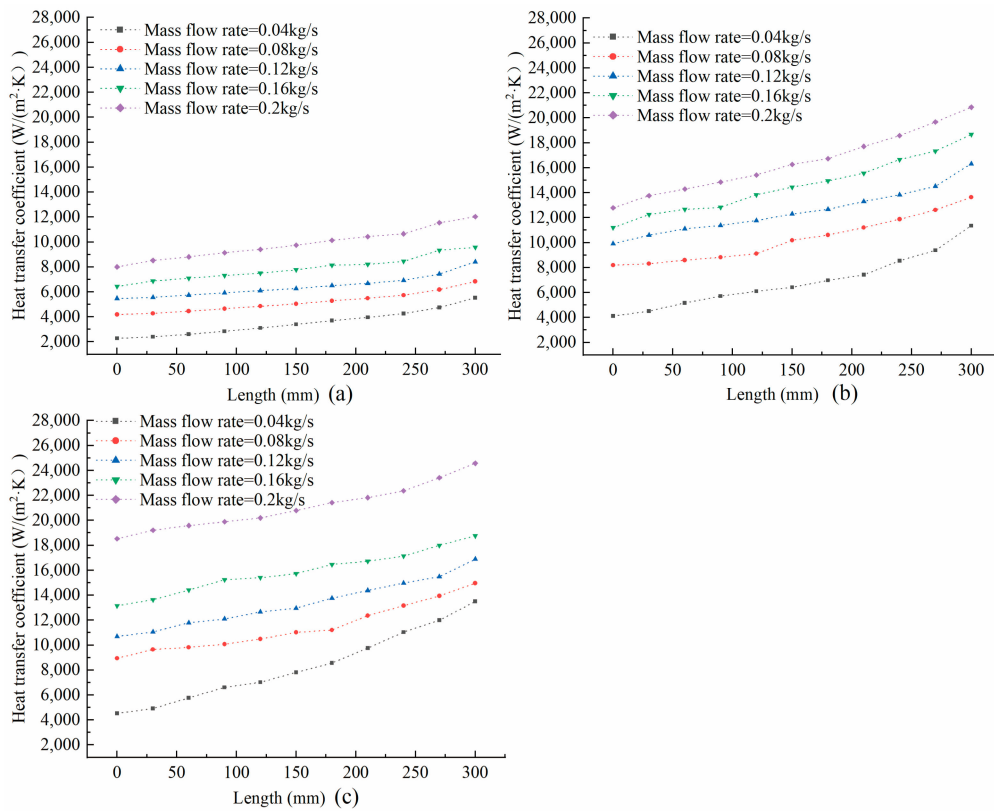


Figure 6. Effect of mass flow rate on the HTC at $T_{\text{water.inlet}} = 320 \text{ K}$ for three different tubes. Smooth tube (a), corrugated tube with circular corrugations (b), and corrugated tube with rectangular corrugations (c).

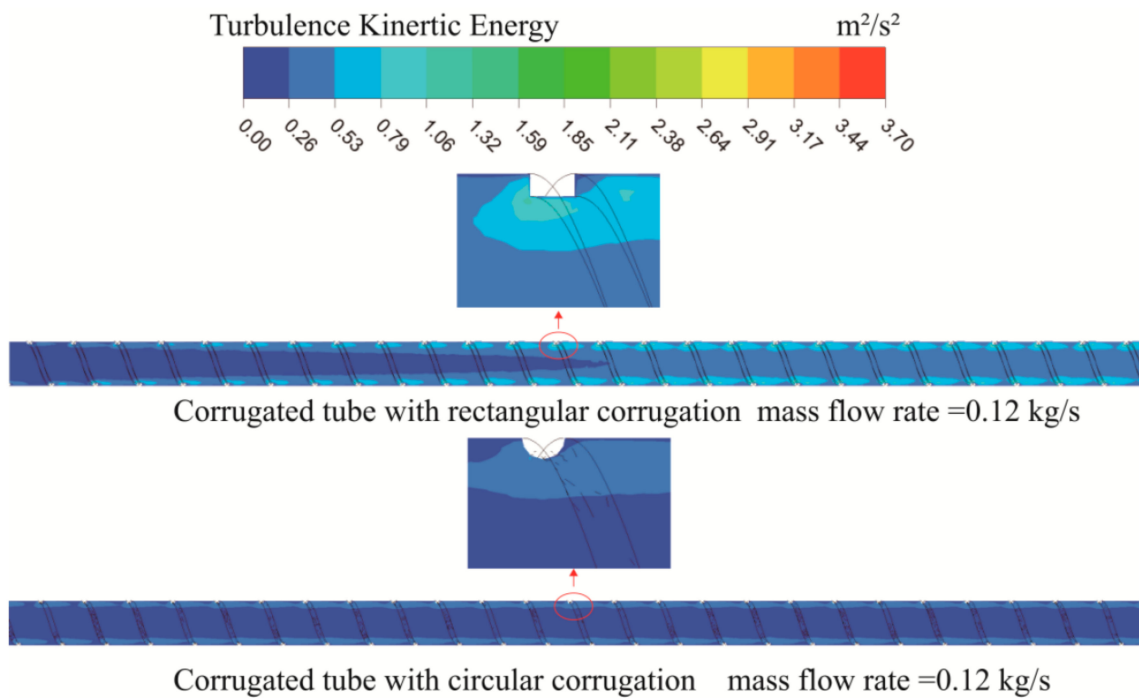


Figure 7. Turbulent kinetic energy of corrugated tubes with circular and rectangular corrugations.

3.1.2. Water Inlet Temperature

The influence of the water inlet temperature on the local HTC in the three different tubes at a constant mass flow rate is shown in Figure 8. The results show that the HTC increases obviously as the distance along the channel increases. However, there is a slight decrease in the HTC as the water inlet temperature increases from 310 K to 330 K [26,30,31]. For one thing, the increase in the water inlet temperature increases the thermal flux at the inner pipe wall. The wall temperature of the internal pipe is increased, leading to the easier formation of nucleation sites. As a result, the bubble formation rate and the number of bubbles grow, resulting in the generation of more R290 vapor. The HTC increases obviously as the distance along the channel increases. Therefore, the amount of R290 vapor increases as the distance along the tube increases, leading to an increase in the HTC with the distance along the tube. This phenomenon is more obvious in corrugated pipes, especially those whose corrugations are rectangular corrugations. For another thing, the increase in the water inlet temperature increases the rate of transition from the liquid to the vapor phase of R290. Due to the convection, the HTC of the vapor is very small compared with the liquid, and the overall HTC in the tube decreases with the generation of more R290 vapor. The reason for this may be that the thermal flow density difference between different water inlet temperatures is small and the impact of the nucleate boiling is lower compared with convection. This phenomenon is more obvious in corrugated tubes due to the corrugated structure that facilitates nucleation boiling and convective heat transfer. Therefore, compared with smooth tubes, corrugated tubes have higher heat transfer coefficients, especially those whose corrugations are rectangular corrugations, which have the highest heat transfer coefficients. The HTC of the corrugated pipe with circular corrugations is 63.2–88.4% higher than that of the smooth pipe, and the HTC of the corrugated pipe with rectangular corrugations is 112.4–132.6% higher than that of the smooth pipe. At the water inlet temperature of 310 K, the HTCs of the corrugated pipe with circular corrugations and the corrugated pipe with rectangular corrugations are the largest, (88.4% and 132.6% higher than those of the smooth pipe, respectively). Therefore, the highest heat transfer efficiency of the corrugated tube is obtained at a lower inlet water temperature (310 K). At the same heat transfer rate, the required heat transfer area of corrugated tubes with circular and rectangular corrugations is 88.4% and 132.6% less than that of smooth tubes, respectively. As a result, the use of corrugated tubes offers the opportunity to reduce the size of the heat exchanger and to reduce the R290 charge in the heat exchanger.

3.2. Pressure Drop

A two-phase flow pressure drop consists of four components: a frictional resistance pressure drop, a local resistance pressure drop, a gravity pressure drop, and an acceleration pressure drop. In this study, the local resistance pressure drop and the gravity pressure drop were not considered due to the simulated pipe being a horizontal smooth pipe. The frictional resistance pressure drop accounts for the largest proportion of the total pressure drop.

3.2.1. Mass Flow Rate

The total pressure drop has a strong dependence on the mass flow rate for all the tubes as illustrated in Figure 9. The mass flow rate of R290 increases, which leads to more wall shear stress. The disturbance of the fluid at the inner tube wall is increased, and the friction between R290 and the internal pipe wall improves, which leads to an increase in the frictional pressure drop. In addition, the acceleration pressure drop that is generated by the different densities and velocities of the R290 gas–liquid phase also increases when the mass flow rate increases. Therefore, the total pressure drop increases as the mass flow rate grows.

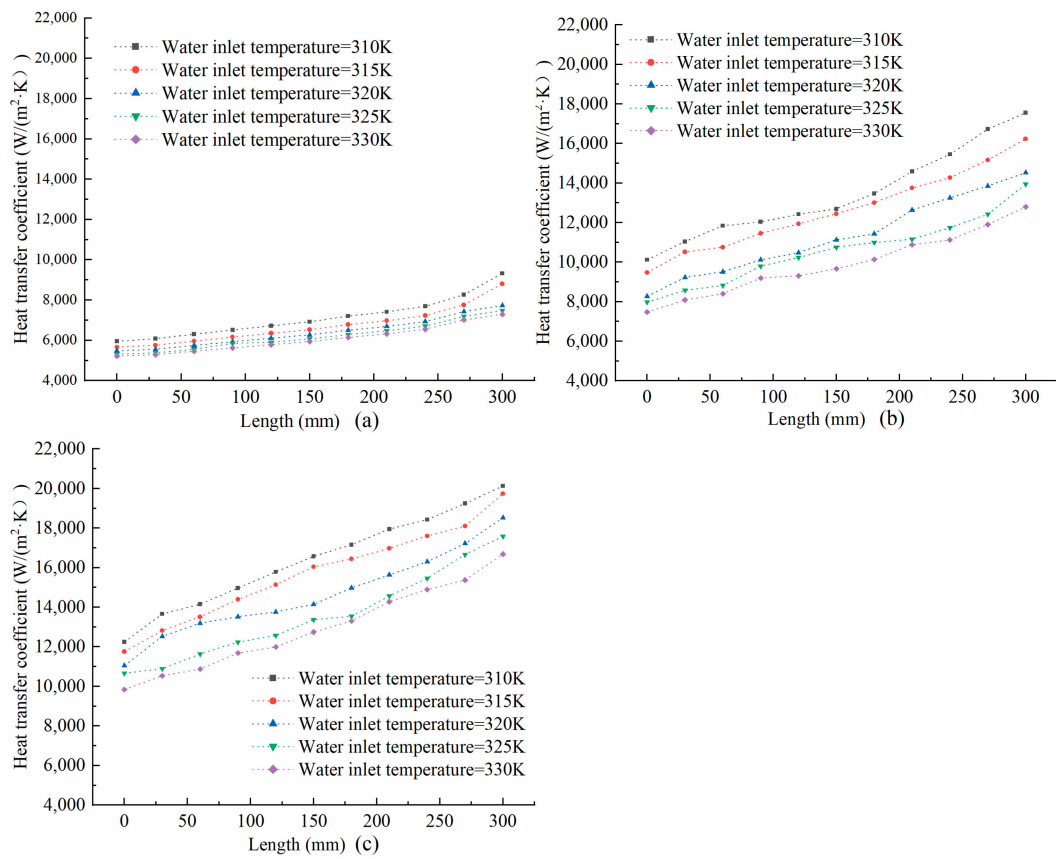


Figure 8. Effect of water inlet temperature on the HTC at a mass flow rate = 0.04 kg/s for the three different tubes. Smooth tube (a), corrugated tube with circular corrugations (b), and corrugated tube with rectangular corrugations (c).

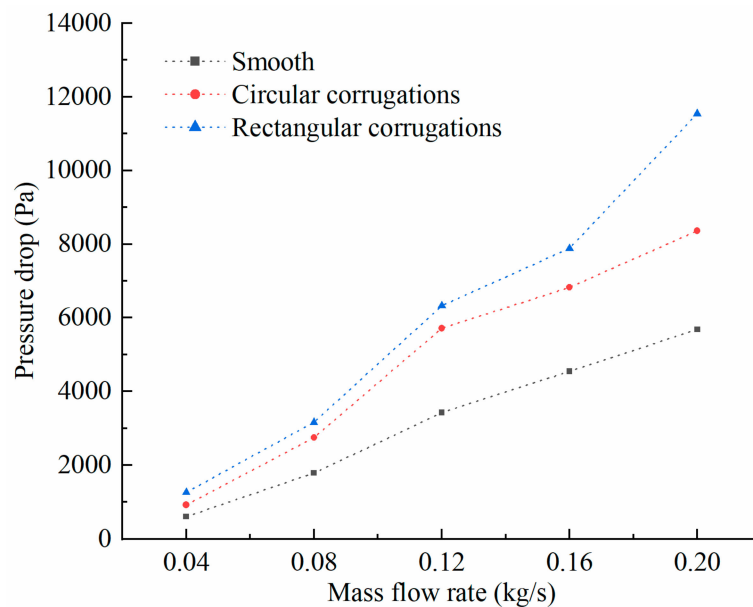


Figure 9. Impact of mass flow rate on the total pressure drop for all the tubes.

This variation happened with the same gradient for both the corrugated and smooth tubes. For the mass flow rate of 0.04–0.20 kg/s, the pressure drop of corrugated tubes whose corrugations are rectangular and circular is 1.73–2.09 and 1.47–1.67 times that of the smooth pipe, respectively. This can be attributed to the fact that the use of corrugated

structures increases the friction surface, which leads to a larger pressure drop. To illustrate the influence of a corrugated structure on the pressure drop, the pressure drop increases along the channel with distance for a constant mass flow rate. The pressure drop is caused by energy dissipation, which is due to fictitious and vortex flow in the fluid flow. Figure 10 shows the fluid gathering and the vortex behavior at the corrugated structure. This phenomenon promotes the turbulent flow of fluids in corrugated pipes, especially those that have rectangular corrugations. Moreover, corrugated tubes have a higher volume fraction of R290 vapor compared with smooth pipes. The density of the liquid–vapor mixture decreases, which leads to an increase in the accelerated pressure drop. As a result, the pressure drop of corrugated tubes is higher compared with smooth tubes.

3.2.2. Water Inlet Temperature

The water inlet temperature does not obviously influence the total pressure drop for all the tubes as shown in Figure 11. The effect of heat flux, which is increased by the water inlet temperature, on shear stress is not significant. This indicates that the friction pressure drop varies slightly with the inlet water temperature. This is one of the reasons for the phenomenon. Compared with the frictional pressure drop, the water inlet temperature has a greater impact on the acceleration pressure drop. The trend of the total pressure drop for the three tubes is more obvious at water inlet temperatures that are higher than 320 K as depicted in Figure 11. The heat flux increases with the water inlet temperature, resulting in an increase in the amount of R290 vapor. The density of the liquid–vapor mixture decreases, which leads to an increase in the accelerated pressure drop. Therefore, the trend of the variation in the total pressure drop at higher water inlet temperatures ($T_{\text{in.water}} > 320 \text{ K}$) is more obvious than at lower water inlet temperatures ($T_{\text{in.water}} < 320 \text{ K}$).

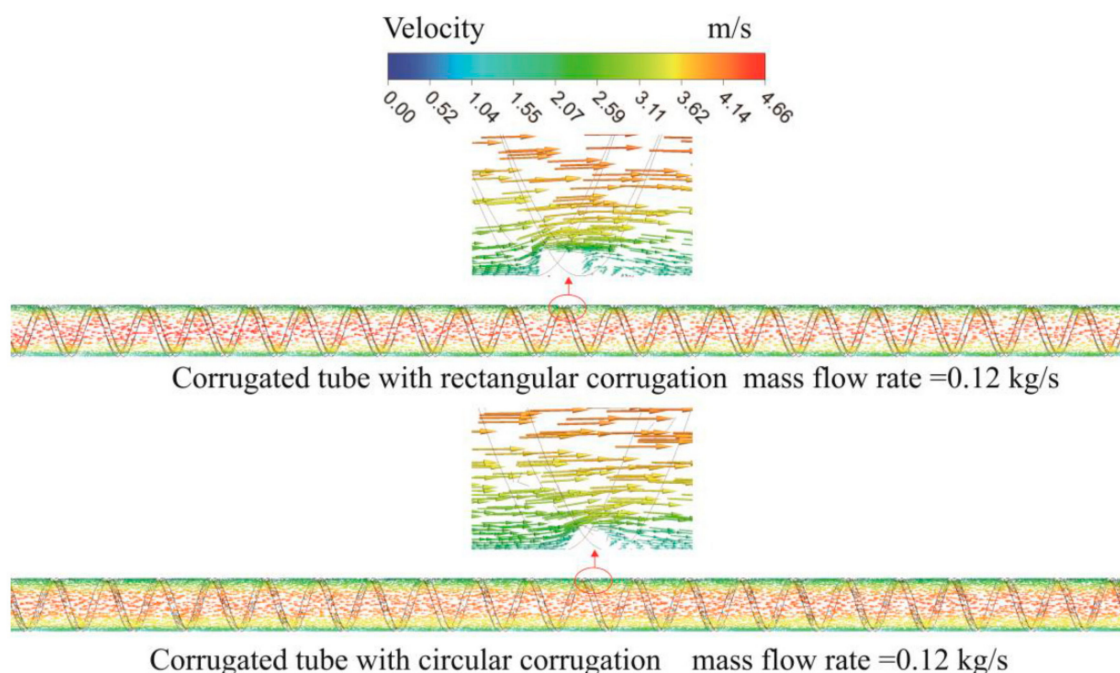


Figure 10. Velocity of the fluid flow in corrugated tubes with circular and rectangular corrugations.

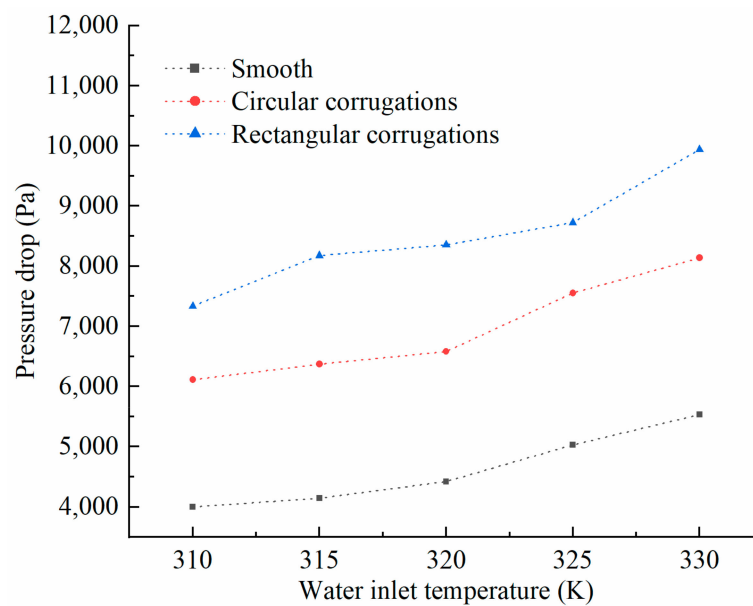


Figure 11. Impact of water inlet temperature on the total pressure drop for all tubes.

This phenomenon happened with the same gradient for both the corrugated and smooth tubes. For the water inlet temperature of 310–330 kg/s, the pressure drop of corrugated tubes whose corrugations are rectangular and circular is 1.74–1.97 and 1.47–1.54 times that of the smooth pipe, respectively. This can be attributed to the fact that the use of corrugated structures increases the friction surface, leading to a larger pressure drop. To indicate the impact of a corrugated structure on the pressure drop, the pressure drop increases along the tube with distance at a constant inlet water temperature. A pressure drop is a change in pressure that is generated by energy dissipation in the fluid flow, such as a friction or a vortex. Figure 10 shows the fluid gathering and the vortex behavior at the corrugated structure. This phenomenon enhances the turbulent flow of fluids in corrugated pipes, especially those that have rectangular corrugations. In addition, corrugated tubes have a higher volume fraction of R290 vapor compared with smooth pipes as shown in Figure 10. The density of the liquid–vapor mixture decreases, causing an increase in the accelerated pressure drop. Thus, the pressure drop of corrugated tubes is higher compared with smooth tubes.

3.3. Effectiveness of Corrugated Tubes

To evaluate the effectiveness of the reinforcement tube for enhanced heat transfer, Colombo et al. [25] defined three parameters: the enhancement factor (E_1), the penalization factor (P_1) and the efficiency index (I). The equations for the three parameters are

$$E_1 = H_{\text{corrugated tube}} / H_{\text{smooth tube}} \quad (21)$$

$$P_1 = \Delta P_{\text{corrugated tube}} / \Delta P_{\text{smooth tube}} \quad (22)$$

$$I = E_f / P_f \quad (23)$$

These values were calculated at a constant water inlet temperature for different mass flow rates as presented in Figure 12. E_1 gradually decreases for the corrugated tube, while P_1 has no significant variation trend over the whole range. As the mass flow rate increases, I shows a downward trend but it is insignificant. This indicates that the rate of increase in the HTC for the smooth tube is higher than that for the corrugated tube as the mass flow rate grows. In addition, the E_1 of the corrugated tube with rectangular corrugations is higher than that of the corrugated tube with circular corrugations, and the E_1 of the corrugated tube with rectangular corrugations and the corrugated tube

with circular corrugations is 2.01–2.36 and 1.67–1.98, respectively. This illustrates that the rectangular corrugated structure enhances the heat transfer more effectively than the circular corrugated structure. However, the P_1 of the corrugated tube with rectangular corrugations is higher than that of the corrugated tube with circular corrugations, and the P_1 of the corrugated tube with rectangular corrugations and the corrugated tube with circular corrugations is 1.73–2.08 and 1.47–1.66, respectively. This indicates that the rectangular corrugated structure causes a higher pressure drop. This is the reason why the I of the corrugated tube with rectangular corrugations is slightly lower than that of the corrugated tube with circular corrugations. The I of the corrugated tube with rectangular corrugations and the corrugated tube with circular corrugations is 1.05–1.24 and 1.13–1.29, respectively. Therefore, corrugated tubes with rectangular corrugations are suited for applications where high heat transfer efficiency is required, while corrugated tubes with circular corrugations are suitable for applications where a low pressure drop is a requirement.

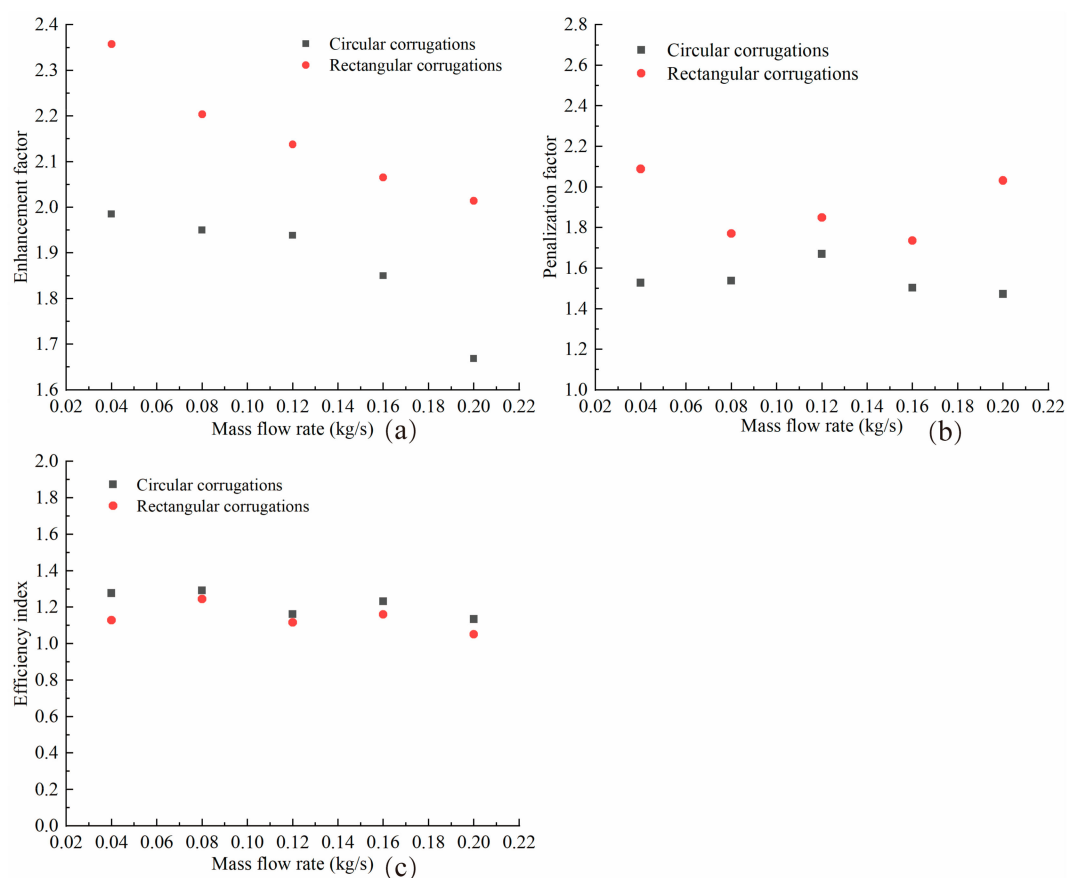


Figure 12. Variations in the enhancement factor E_1 (a), penalization factor P_1 (b), and efficiency index I (c) with mass flow rate.

4. Conclusions

The flow boiling of R290 in a smooth pipe and two corrugated pipes with a 5 mm ID was investigated by numerical simulation in this study. The numerical simulation of the three-dimensional model was verified with the Liu–Winterton and Xu–Fang empirical equations. The HTC and pressure drop were obtained at saturation temperatures ranging between 273 and 283 K for the smooth tube, while the HTC and pressure drop were compared for the three tubes at a mass flow rate ranging from 0.04 to 0.2 kg/s and a water inlet temperature ranging from 310 K to 330 K. In addition, E_1 , P_1 , and I were utilized to evaluate the effectiveness of the enhanced heat transfer of the two corrugated tubes. The main conclusions of this study can be summarized as follows:

- (1) The HTC and pressure drop slightly vary with the saturation temperature. As the mass flow rate increases, the HTC and pressure drop of the corrugated tube obviously increase over the whole tube compared with the smooth tube. As the water inlet temperature increases, the HTC decreases over the whole tube for each of the three tubes.
- (2) The E_1 and P_1 of the corrugated pipe with rectangular corrugations are higher than those of the corrugated pipe with circular corrugations. The E_1 of the corrugated tube with rectangular corrugations and the corrugated tube with circular corrugations is 2.01–2.36 and 1.67–1.98, respectively. The corrugated structure enhances the heat transfer significantly. The P_1 of the corrugated tube with rectangular corrugations and the corrugated tube with circular corrugations is 1.73–2.08 and 1.47–1.66, respectively. The I of the corrugated pipe with rectangular corrugations is slightly lower than that of the corrugated pipe with circular corrugations. The I of the corrugated tube with rectangular corrugations and the corrugated tube with circular corrugations is 1.05–1.24 and 1.13–1.29, respectively.
- (3) The corrugated tubes with rectangular corrugations are best suited for applications where high heat transfer efficiency is required, while corrugated tubes with circular corrugations are suitable for applications where a low pressure drop is required.
- (4) At the same heat transfer rate, the required heat transfer area of corrugated tubes with circular and rectangular corrugations is 63.2–98.5% and 101.4–135.7% less than that of smooth tubes, respectively. Therefore, the use of corrugated tubes provides an opportunity to reduce the size of heat exchangers and to reduce the material cost of manufacturing heat exchangers.

Author Contributions: S.Z.: conceptualization, formal analysis, data curation, writing—original draft, review, and editing. J.W.: conceptualization, funding acquisition, supervision, writing—original draft, review, and editing. J.X.: conceptualization, funding acquisition, supervision, writing—original draft, review, and editing. All authors have read and agreed to the published version of the manuscript.

Funding: This research was supported by the Science and Technology Innovation Action Plan of the Shanghai Science and Technology Commission (19DZ1207503) and the Public Service Platform Project of the Shanghai Science and Technology Commission (20DZ2292200).

Institutional Review Board Statement: Not applicable.

Informed Consent Statement: Not applicable.

Data Availability Statement: Not applicable.

Acknowledgments: This research was supported by the Science and Technology Innovation Action Plan of the Shanghai Science and Technology Commission (19DZ1207503) and the Public Service Platform Project of the Shanghai Science and Technology Commission (20DZ2292200).

Conflicts of Interest: The authors declare no conflict of interest.

Abbreviations

Nomenclature

E	Energy, j
E_1	Enhancement factor
E_f	Enhancement factor
F	Body force, N
G	Generation of turbulence K. E
g	Gravity, m/s ²
h	Enthalpy, kg/j
H	Transfer heat coefficient

Greek letters

ρ	Density, kg/m ³
μ	Viscosity, kg/m s
α	Volume fraction
ε	Dissipation rate
∇	Surface gradient operator
λ	thermal conductivity

Subscripts

dr	Drift
------	-------

I	Efficiency index	l	Liquid
K	Kinetic energy, j	v	Vapor
L	Length, m	m	Mixture
M	Mach number	k	Phase
P	Pressure, Pa	p	Primary phase
P_1	Penalization factor	q	Secondary phase
Pr	Prandtl number	w	Wall
Q	Heat flux, W/m^2	sat	Saturation
Re	Reynolds number	s	Source
Sf	Suppression factor	Abbreviations	
S	Modulus of the mean rate-of-strain tensor	CFD	Computational fluid dynamics
T	Temperature, K	HTC	Heat transfer coefficient
t	Time, s	ODP	Ozone Depletion Potential
v	Velocity, m/s	GWP	Global Warming Potential
		ID	Inner diameter

References

- Bolaji, B.O.; Huan, Z. Ozone depletion and global warming: Case for the use of natural refrigerant—A review. *Renew. Sustain. Energy Rev.* **2013**, *18*, 49–54. [\[CrossRef\]](#)
- Choudhari, C.S.; Sapali, S.N. Performance Investigation of Natural Refrigerant R290 as a Substitute to R22 in Refrigeration Systems. *Energy Procedia* **2017**, *109*, 346–352. [\[CrossRef\]](#)
- Jierong, L.; Tingxun, L. Detailed dynamic refrigerant migration characteristics in room air-conditioner with R290. *Int. J. Refrig.* **2018**, *88*, 108–116. [\[CrossRef\]](#)
- Jawale, V.S.; Keche, A.J. Experimental performance study of R290 as an alternative to R22 refrigerant in a window air conditioner. In *IOP Conference Series: Materials Science and Engineering*; IOP Publishing: Bristol, UK, 2018; Volume 377.
- Nawaz, K.; Shen, B.; Elatar, A.; Baxter, V.; Abdelaziz, O. R290 (propane) and R600a (isobutane) as natural refrigerants for residential heat pump water heaters. *Appl. Therm. Eng.* **2017**, *127*, 870–883. [\[CrossRef\]](#)
- Allymehr, E.; Pardiñas, Á.Á.; Eikevik, T.M.; Hafner, A. Characteristics of evaporation of propane (R290) in compact smooth and microfinned tubes. *Appl. Therm. Eng.* **2020**, *181*, 115880. [\[CrossRef\]](#)
- Lillo, G.; Mastrullo, R.; Mauro, A.W.; Viscito, L. Flow boiling heat transfer, dry-out vapor quality and pressure drop of propane (R290): Experiments and assessment of predictive methods. *Int. J. Heat Mass Transf.* **2018**, *126*, 1236–1252. [\[CrossRef\]](#)
- Zhou, W.; Gan, Z. A potential approach for reducing the R290 charge in air conditioners and heat pumps. *Int. J. Refrig.* **2019**, *101*, 47–55. [\[CrossRef\]](#)
- Chien, N.B.; Vu, P.Q.; Choi, K.-I.; Oh, J.-T. Boiling Heat Transfer of R32, CO₂ and R290 inside Horizontal Minichannel. *Energy Procedia* **2017**, *105*, 4822–4827. [\[CrossRef\]](#)
- Zhou, S.; Zhao, X.; Cai, D.; Deng, J.; Gao, Y.; He, G. Experimental evaluation on flow boiling heat transfer of R290/POE-oil working fluid for absorption refrigeration in smooth horizontal tubes. *Int. J. Therm. Sci.* **2021**, *159*, 106641. [\[CrossRef\]](#)
- de Oliveira, J.D.; Passos, J.C.; Copetti, J.B.; van der Geld, C.W.M. Flow boiling heat transfer of propane in 1.0 mm tube. *Exp. Therm. Fluid Sci.* **2018**, *96*, 243–256. [\[CrossRef\]](#)
- Andreozzi, A.; Manca, O.; Nardini, S.; Ricci, D. Forced convection enhancement in channels with transversal ribs and nanofluids. *Appl. Therm. Eng.* **2016**, *98*, 1044–1053. [\[CrossRef\]](#)
- Liu, L.; Cao, Z.; Shen, T.; Zhang, L.; Zhang, L. Experimental and numerical investigation on flow and heat transfer characteristics of a multi-waves internally spiral finned tube. *Int. J. Heat Mass Transf.* **2021**, *172*, 121104. [\[CrossRef\]](#)
- Zhang, S.; Xu, X.; Liu, C.; Wu, C.; Sun, P.; Dang, C. Experimental investigation of the heat transfer behaviors of CO₂, propane and their binary non-azeotropic mixtures above critical pressure in helically coiled tube. *Appl. Therm. Eng.* **2020**, *180*, 115842. [\[CrossRef\]](#)
- Gururatana, S.; Skullong, S. Heat transfer augmentation in a pipe with 3D printed wavy insert. *Case Stud. Therm. Eng.* **2020**, *21*, 100698. [\[CrossRef\]](#)
- Vaisi, A.; Moosavi, R.; Lashkari, M.; Mohsen Soltani, M. Experimental investigation of perforated twisted tapes turbulator on thermal performance in double pipe heat exchangers. *Chem. Eng. Process.-Process. Intensif.* **2020**, *154*, 108028. [\[CrossRef\]](#)
- Tokgoz, N.; Aksoy, M.M.; Sahin, B. Investigation of flow characteristics and heat transfer enhancement of corrugated duct geometries. *Appl. Therm. Eng.* **2017**, *118*, 518–530. [\[CrossRef\]](#)
- Job, V.M.; Gunakala, S.R. Mixed convective ferrofluid flow through a corrugated channel with wall-mounted porous blocks under an alternating magnetic field. *Int. J. Mech. Sci.* **2018**, *144*, 357–381. [\[CrossRef\]](#)
- Manjunath, M.S.; Karanth, K.V.; Sharma, N.Y. Numerical investigation on heat transfer enhancement of solar air heater using sinusoidal corrugations on absorber plate. *Int. J. Mech. Sci.* **2018**, *138–139*, 219–228. [\[CrossRef\]](#)

20. Ajeel, R.K.; Salim, W.S.I.W.; Hasnan, K. Design characteristics of symmetrical semicircle-corrugated channel on heat transfer enhancement with nanofluid. *Int. J. Mech. Sci.* **2019**, *151*, 236–250. [[CrossRef](#)]
21. Navickaitė, K.; Cattani, L.; Bahl, C.R.H.; Engelbrecht, K. Elliptical double corrugated tubes for enhanced heat transfer. *Int. J. Heat Mass Transf.* **2019**, *128*, 363–377. [[CrossRef](#)]
22. Córcoles, J.I.; Moya-Rico, J.D.; Molina, A.E.; Almendros-Ibáñez, J.A. Numerical and experimental study of the heat transfer process in a double pipe heat exchanger with inner corrugated tubes. *Int. J. Therm. Sci.* **2020**, *158*, 106526. [[CrossRef](#)]
23. Diani, A.; Rossetto, L. R513A flow boiling heat transfer inside horizontal smooth tube and microfin tube. *Int. J. Refrig.* **2019**, *107*, 301–314. [[CrossRef](#)]
24. Celen, A.; Çebi, A.; Dalkılıç, A.S. Investigation of boiling heat transfer characteristics of R134a flowing in smooth and microfin tubes. *Int. Commun. Heat Mass Transf.* **2018**, *93*, 21–33. [[CrossRef](#)]
25. Colombo, L.P.M.; Lucchini, A.; Muzzio, A. Flow patterns, heat transfer and pressure drop for evaporation and condensation of R134A in microfin tubes. *Int. J. Refrig.* **2012**, *35*, 2150–2165. [[CrossRef](#)]
26. Mohammed, H.I.; Giddings, D.; Walker, G.S. CFD multiphase modelling of the acetone condensation and evaporation process in a horizontal circular tube. *Int. J. Heat Mass Transf.* **2019**, *134*, 1159–1170. [[CrossRef](#)]
27. Alazwari, M.A.; Safaei, M.R. Combination Effect of Baffle Arrangement and Hybrid Nanofluid on Thermal Performance of a Shell and Tube Heat Exchanger Using 3-D Homogeneous Mixture Model. *Mathematics* **2021**, *9*, 881. [[CrossRef](#)]
28. Liu, Z.; Winterton, R.H.S. A general correlation for saturated and subcooled flow boiling in tubes and annuli, based on a nucleate pool boiling equation. *Int. J. Heat Mass Transf.* **1991**, *34*, 2759–2766. [[CrossRef](#)]
29. Xu, Y.; Fang, X. A new correlation of two-phase frictional pressure drop for evaporating flow in pipes. *Int. J. Refrig.* **2012**, *35*, 2039–2050. [[CrossRef](#)]
30. Magnini, M.; Thome, J.R. A CFD study of the parameters influencing heat transfer in microchannel slug flow boiling. *Int. J. Therm. Sci.* **2016**, *110*, 119–136. [[CrossRef](#)]
31. Yu, J.; Ma, H.; Jiang, Y. A numerical study of heat transfer and pressure drop of hydrocarbon mixture refrigerant during boiling in vertical rectangular minichannel. *Appl. Therm. Eng.* **2017**, *112*, 1343–1352. [[CrossRef](#)]